Research Article

Identification of key genes involved in axon regeneration and Wallerian degeneration by weighted gene co-expression network analysis

https://doi.org/10.4103/1673-5374.322473

Date of submission: January 15, 2021

Date of decision: April 12, 2021

Date of acceptance: July 8, 2021

Date of web publication: August 30, 2021

Yan Lu[1, #], Qi Shan[1, #], Mei Ling[2], Xi-An Ni[1], Su-Su Mao[1], Bin Yu[1, *], Qian-Qian Cao[1, *]

Graphical Abstract *Identification of Kif22 as a key regulator of sciatic nerve repair*

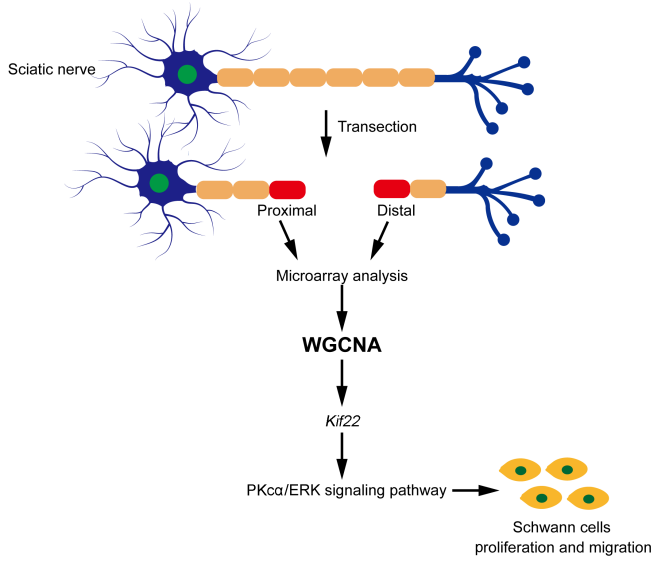

Abstract

Peripheral nerve injury repair requires a certain degree of cooperation between axon regeneration and Wallerian degeneration. Therefore, investigating how axon regeneration and degeneration work together to repair peripheral nerve injury may uncover the molecular mechanisms and signal cascades underlying peripheral nerve repair and provide potential strategies for improving the low axon regeneration capacity of the central nervous system. In this study, we applied weighted gene co-expression network analysis to identify differentially expressed genes in proximal and distal sciatic nerve segments from rats with sciatic nerve injury. We identified 31 and 15 co-expression modules from the proximal and distal sciatic nerve segments, respectively. Functional enrichment analysis revealed that the differentially expressed genes in proximal modules promoted regeneration, while the differentially expressed genes in distal modules promoted neurodegeneration. Next, we constructed hub gene networks for selected modules and identified a key hub gene, *Kif22*, which was up-regulated in both nerve segments. *In vitro* experiments confirmed that *Kif22* knockdown inhibited proliferation and migration of Schwann cells by modulating the activity of the extracellular signal-regulated kinase signaling pathway. Collectively, our findings provide a comparative framework of gene modules that are co-expressed in injured proximal and distal sciatic nerve segments, and identify *Kif22* as a potential therapeutic target for promoting peripheral nerve injury repair via Schwann cell proliferation and migration. All animal experiments were approved by the Institutional Animal Ethics Committee of Nantong University, China (approval No. S20210322-008) on March 22, 2021.

Key Words: axon regeneration; extracellular signal-regulated kinase signaling pathway; hub genes; *Kif22*; peripheral nerve injury; protein kinase Cα; Schwann cells; Wallerian degeneration; weighted gene co-expression network analysis

Chinese Library Classification No. R446; R745; Q344+.12

[1]Key Laboratory of Neuroregeneration of Jiangsu and Ministry of Education, Co-innovation Center of Neuroregeneration, Nantong University, Nantong, Jiangsu Province, China; [2]School of Life Sciences, Nantong University, Nantong, Jiangsu Province, China

*__Correspondence to:__ Qian-Qian Cao, PhD, cqq09100239@163.com; Bin Yu, PhD, yubin@ntu.edu.cn

https://orcid.org/0000-0002-9677-6916 (Qian-Qian Cao); https://orcid.org/0000-0002-8927-3333 (Bin Yu)

#Both authors contributed equally to the work.

Funding: *This study was supported by the National Major Project of Research and Development of China, No. 2017YFA0104701 (to BY); the National Natural Science Foundation of China, No. 32000725 (to QQC); the Natural Science Foundation of Jiangsu Province of China, No. BK20200973 (to QQC); and the Jiangsu Provincial University Innovation Training Key Project of China, No. 202010304021Z (to ML).*

How to cite this article: *Lu Y, Shan Q, Ling M, Ni XA, Mao SS, Yu B, Cao QQ (2022) Identification of key genes involved in axon regeneration and Wallerian degeneration by weighted gene co-expression network analysis. Neural Regen Res 17(4):911-919.*

Introduction

Peripheral nerve injury often occurs during surgery, and refers to primary or secondary lesions within the peripheral nervous system. Trauma, tumor, metabolic disease, and other factors can induce peripheral nerve injury, leading to sensory, motor, and nutritional disorders in the innervated region. Unlike the central nervous system, the peripheral nervous system has regenerative capacity, which involves an orderly series of morphological and molecular events that lead to repair following injury (He and Jin, 2016). Injury that severs a nerve completely results in division of the axon into proximal and distal nerve stumps: the nerve stump connected to the cell body is referred to as the proximal axon segment, and the disconnected nerve stump is referred to as the distal axon segment (Girouard et al., 2018). After peripheral nerve injury, the axon begins to regenerate from the proximal stump, while the distal stump undergoes Wallerian degeneration (WD) (Coleman and Freeman, 2010; Girouard et al., 2018).

In recent years, considerable progress has been made in understanding the mechanism of peripheral nerve repair (He and Jin, 2016; Mahar and Cavalli, 2018). In particular, the intrinsic molecular mechanisms that separately underlie axon regeneration and degeneration are now well understood (Coleman and Freeman, 2010; Conforti et al., 2014; Mahar and Cavalli, 2018). However, proximal axon regeneration and distal degeneration are not completely independent processes. A previous study showed that successful nerve repair requires a degree of coordination between axon regeneration and WD (Girouard et al., 2018). Degeneration of the distal axon segment creates conditions that induce axon regrowth from proximal stumps, thus influencing the regenerative capacity of the proximal axon segment. In addition, several molecules, such as Dual leucine zipper kinase, c-Jun N-terminal kinase, calpain, stathmin 2, and nicotinamide nucleotide adenylyltransferase 2, and some cellular processes, including Schwann cell (SC) dedifferentiation and proliferation, axonal transport, mitochondrial dynamics, and cytoskeletal dynamics have been shown to play essential roles in both axon regeneration and degeneration (Jessen and Mirsky, 2016; Prior et al., 2017; Blanquie and Bradke, 2018; Girouard et al., 2018; Smith and Gallo, 2018). Therefore, investigating how axon regeneration and degeneration work together to regulate peripheral injury repair may not only reveal the molecular mechanisms and signal cascades involved in peripheral nerve repair, but also suggest potential strategies to improve proximal axon segment regeneration in the central nervous system, which lacks regenerative capacity.

To understand how axon regeneration and degeneration work together to regulate peripheral injury repair, we sought to generate a comprehensive framework of gene expression in proximal and distal nerve segments. Microarray and RNA-sequencing, two emerging high-throughput sequencing technologies, were used to systematically monitor gene expression profile changes during axonal regeneration and degeneration, respectively. Previous work from our group used microarray analysis to reveal transcriptome alterations in the proximal and distal segments of sciatic nerves undergoing WD (Yao et al., 2013; Jiang et al., 2014; Yu et al., 2016; Yi et al., 2017). However, these earlier studies did not systematically analyze and compare gene expression profiles between the proximal and distal nerve segments. To address this, in the current study we applied weighted gene co-expression network analysis (WGCNA), an efficient and accurate bioinformatics and biological data mining method, along with a comprehensive collection of R functions that are used to perform various aspects of weighted correlation network analysis, and frequently to analyze interactions between genes and phenotypes (Zhang and Horvath, 2005; Liu et al., 2017). WGCNA can help compare differentially expressed genes, as well as identify relationships among genes in different co-expression modules (Liu et al., 2017; Wan et al., 2018). The aim of the current study was to use WGCNA to compare co-expression gene modules between proximal and distal nerve segments and to identify genes that play key roles in regulating peripheral nerve repair.

Kinesin family member 22 (*Kif22*) encodes a motor protein that transports organelles within cells and moves chromosomes during cell division. *Kif22* has been previously reported to regulate extracellular signal-regulated kinase (ERK) signal pathway-induced cell proliferation and migration, as well as epidermal growth factor receptor signaling (Yu et al., 2014, 2020; Pike et al., 2018). Given that cell division, proliferation, and migration are essential for nerve repair and that the ERK and epidermal growth factor receptor signaling pathways play important roles in nerve repair (Zhou and Li, 2007; Napoli et al., 2012), we investigated whether *Kif22* plays a role in peripheral nerve injury repair.

Materials and Methods

Animal surgery and tissue collection

Changing estrogen levels in female mice would have interfered with analysis of gene expression after nerve injury, so only male mice were used in this study. One hundred and forty-seven adult male Sprague-Dawley rats (specific-pathogen-free level, 8-week-old, weighing 160–200 g) were provided by the Experimental Animal Center of Nantong University (license Nos. SYXK (Su) 2014-0001 and SYXK (Su) 2017-0046). All animals were maintained and used in accordance with the guidelines of Institutional Animal Care of Nantong University. All animal experiments were approved by the Institutional Animal Ethics Committee of Nantong University, China (approval No. S20210322-008) on March 22, 2021. The rats were randomly divided into seven groups (0-, 1-, and 6-hour and 1-, 4-, 7-, and 14-day groups), each of which included six rats. All of the rats were subjected to sciatic nerve transection surgery, as previously described (Jiang et al., 2014). Briefly, the sciatic nerve was exposed through an incision in the midlateral area of the thigh of the left hind leg, and a 10-mm nerve segment was excised. At 0, 1, or 6 hours or 1, 4, 7, or 14 days post-surgery, the rats were sacrificed by abdominal injection of a mixture of 85 mg/kg trichloroacetaldehyde monohydrate (Lingfeng Chemical Reagent, Shanghai, China), 42 mg/kg magnesium sulfate (Lingfeng Chemical Reagent), and 17 mg/kg sodium pentobarbital (Millipore Sigma, Burlington, MA, USA), and 0.5-cm segments of the proximal and distal nerve stumps were harvested.

Microarray analysis

Microarray analysis was carried out as previously described (Yi et al., 2017). Total RNA was extracted from the proximal and distal nerve segments of rats with sciatic nerve injury using Trizol reagent (Sigma, San Francisco, CA, USA) according to the manufacturer's instructions. RNeasy spin columns (Qiagen, Valencia, CA, USA) were used to remove contaminating DNA. Then, RNA quality assessment, amplification, labeling, hybridization, and further microarray analysis of each sample were conducted by the Shanghai Biotechnology Corporation, Shanghai, China. Three biological replicates were included for each group.

Weighted gene co-expression network analysis

WGCNA was carried out using the WGCNA R software package (https://horvath.genetics.ucla.edu/html/

CoexpressionNetwork/Rpackages/WGCNA/). Differentially expressed genes identified by microarray analysis were then subjected to co-expression network analysis. First, we filtered out genes with low variation in expression (standard deviation ≤ 0.25). Then, we used a Pearson correlation matrix to perform co-expression analysis of paired genes. We selected an adjacency matrix weight parameter power of 14, based on a previous report, to satisfy the preconditions of scale-free network distribution as much as possible. Finally, based on this selected power value, we established a weighted co-expression network model that divided the differentially expressed genes in the proximal and distal groups into 31 and 15 modules, respectively.

Identification of significant modules and key genes

To identify the important modules, a Pearson correlation algorithm was applied to compute the correlation coefficient and *P* value of module characteristic genes and trait (time post-injury). Then, an absolute correlation coefficient value ≥ 0.5 and a *P* value < 0.05 were used as thresholds to screen for modules related to the trait. Once the modules of interest were selected, the correlation between module gene expression and corresponding traits (gene significance, GS), as well as the correlation between module gene expression and module characteristic gene (module membership, MM) was calculated for each important gene. Then, thresholds of MM > 0.9 and GS > 0.5 were used to identify key genes in the indicated modules.

Functional enrichment analysis of co-expression modules

Genes in the selected modules were subjected to functional enrichment analysis with corresponding databases. The Gene Ontology database (GO, http://geneontology.org/) was used to identify genes and gene enrichment, and the Kyoto Encyclopedia of Genes and Genomes database (KEGG, http://www.genome.jp/kegg/) was used for pathway analysis. A threshold of *P* value ≤ 0.05 was used to define significant GO categories and KEGG pathways, and the top ten records were extracted for each analysis. Cytoscape software (https://cytoscape.org/) was applied to further visualize the modules of interest, and the 50 genes with the greatest intramodular connectivity were identified as hub genes.

Quantitative real-time polymerase chain reaction

Total RNA was isolated from nerve tissues and SCs using TRizol reagent from Sigma. The RNA was treated with RNase-free DNase I and reverse transcribed with a Prime-Script RT Kit (TaKaRa, Dalian, China) according to the manufacturer's instructions. Quantitative real-time polymerase chain reaction was performed with the SYBR Premix Ex Taq (TaKaRa). Glyceraldehyde-3-phosphate dehydrogenase (*GAPDH*) was used as an internal control to normalize mRNA expression. The primers used are listed in **Additional Table 1**.

Schwann cells primary culture and transfection

Primary SCs were isolated, maintained, and transfected as previously described (Yao et al., 2016). Sciatic nerves were harvested from seven 1-day-old Sprague-Dawley rats (specific-pathogen-free) from the Experimental Animal Center of Nantong University and used to isolate SCs, which were then purified with anti-Thy1.1 antibody (mouse, 1:1000, Cat# M7898, Sigma-Aldrich, St. Louis, MO, USA) and rabbit complement (25%, Cat# 31024100, Invitrogen, Carlsbad, CA, USA) to remove the fibroblasts. The purified SCs were maintained in Dulbecco's modified Eagle medium (Gibco, Grand Island, NY, USA) containing 10% fetal bovine serum (Gibco) at 37°C under humidified conditions with 5% CO_2.

Primary cultured SCs were transfected with a negative control small interfering RNA (siRNA) or a *Kif22*-specific siRNA (Ribobio, Guangzhou, China) using Lipofectamine RNAiMAX transfection reagent (Invitrogen), as previously described (Yao et al., 2016). The target sequences of the siRNA duplexes were as follows: *Kif22*-specific siRNA-1, 5′-CCT GAA GAA AGG CCA CAA A-3′; *Kif22*-specific siRNA-2, 5′-CCA TCA CTA GCT TCT CTG A-3′; *Kif22*-specific siRNA-3, 5′-GTG ATT AAC CGG CCT TTC A-3′; negative control siRNA, 5′-GGC UCU AGA AAA GCC UAU GC-3′.

5-Ethynyl-2′-deoxyuridine proliferation assay

SC proliferation was analyzed using a 5-ethynyl-2′-deoxyuridine (EdU) cell proliferation kit (Ribobio). The SCs transfected with the indicated siRNA were seeded into a 96-well culture plate at a density of 1×10^5 cells/well and incubated with 50 μM EdU for 4 hours. Next, the treated SCs were fixed in 4% paraformaldehyde for 30 minutes and permeabilized with Triton X-100 for 15 minutes. Then, the cells were stained with Apollo fluorescent dye, and the cell nuclei were stained with 5 μg/mL Hoechst 33342, for 20 minutes. The ratio of EdU-positive to total cells was calculated using ImageJ software (National Institutes of Health, Bethesda, MD, USA) from four randomly selected images photographed under a Olympus fluorescence microscope (Shinjuku, Tokyo, Japan). The EdU assay was carried out in triplicate, with three identical wells included for each sample.

Transwell assay

SC migration was detected using Transwell chambers (Corning, New York, NY, USA) with a diameter of 6.5 mm and with 8 μm pores, as previously reported (Yao et al., 2016). The bottom membrane of each chamber was coated with 5 μg/mL fibronectin (Millipore, Billerica, MA, USA) three times before use. Then, primary SCs resuspended in 100 μL Dulbecco's modified Eagle medium (1×10^6 cells/mL) were seeded to the upper chambers and 500 μL complete medium (Dulbecco's modified Eagle medium with 10% fetal bovine serum) was added to the lower chambers. At the indicated time point, the cells were fixed with 4% paraformaldehyde for 30 minutes, and the cells that were adhered to the bottom chamber were stained with 0.1% crystal violet for 15 minutes. Next, the remaining crystal violet solution was remove by rinsing with sterile water, the cells were gently swabbed off of the upper chamber using a cotton swab. The stained cells were imaged under a Olympus fluorescence microscope. Finally, a 33% acetic acid solution was applied to dissolve the crystal violet, and a Synergy 2 multifunctional detector (BioTek, Burlington, VT, USA) was further used to detect the absorbance at 570 nm to quantify the migrated cells. Each experiment was performed in triplicate.

Wound healing assay

A wound healing assay was carried out using a Culture-Insert 2 Well in μ-Dish 35 mm (iBidi, Gräfelfing, Germany). The culture inserts were placed in 6-well plates before use. Then, SCs transfected with the indicated siRNA were seeded into the two wells of the culture inserts and maintained for 24 hours. Next, the culture inserts were removed to expose the blank area (or "wound") between the two wells, which was photographed to serve as the control (0 hour) image. The remaining cells were starved in Dulbecco's modified Eagle medium supplemented with 5% fetal bovine serum and 0.15 μg/mL mitomycin C (Sigma) for 12 hours. Finally, cells migrating across the wound in four randomly selected fields were photographed, and the percentage of wound healing (relative to the control image) was measured and analyzed using ImageJ software at the indicated time points. Three independent wells were included for each sample.

Western blot analysis

SCs transfected with the indicated siRNAs (*Kif22*-specific siRNAs or negative control siRNA) were lysed with a buffer containing protease and phosphatase inhibitors to extract total protein. The extracted proteins were subjected to electrophoresis on a 10% sodium dodecyl sulfate-polyacrylamide gel and then transferred to a nitrocellulose membrane (Merck Millipore, Billerica, MA, USA). Next, the membranes were incubated with anti-ERK (rabbit, 1:1000, Cat# A4782, Abclonal, Boston, MA, USA), anti-p-ERK (phospho-ERK1-T202/Y204 + ERK2-T185/Y187, rabbit, 1:1000, Cat# AP0974, Abclonal), anti-protein kinase C α (PKCα; rabbit, 1:1000, Cat# A11107, Abclonal), and anti-GAPDH (rabbit, 1:2500, Cat# G9545, Sigma) antibodies at 4°C overnight. Then, the samples were incubated with goat anti-rabbit IgG-horseradish peroxidase (1:1000, Cat# abs20040, Absin Bioscience Inc, Shanghai, China) at room temperature for 2 hours. The blot images were scanned using a Tanon5200multi system (Tanon, Shanghai, China). Finally, quantitative analysis was performed using ImageJ software. Protein levels were normalized to GAPDH.

Statistical analysis

Unpaired *t*-test was performed for all statistical analyses using GraphPad Prism 9 (GraphPad Software, San Diego, CA, USA). A P value < 0.05 was considered statistically significant, and all results are shown as mean ± standard deviation.

Results

Construction of co-expression modules for proximal and distal nerve segments from rats with sciatic nerve injury

To systematically analyze and compare gene expression between proximal and distal nerve segments, we first performed a microarray analysis and found that there were 17,482 and 13,988 differentially expressed genes at 0, 1, and 6 hours, and 1, 4, 7, and 14 days post-sciatic nerve transection in the proximal and distal nerve stumps, respectively. We then used WGCNA, a method for transforming gene expression data into co-expression modules, to separately analyze the differentially expressed genes in the proximal and distal nerve stumps. Before constructing the co-expression modules, we filtered out differentially expressed genes with low expression variation (standard deviation ≤ 0.25), yielding 13,331 proximal and 10,726 distal genes. Power value is another critical parameter that affects the independence and average degree of connectivity of co-expression modules. Hence, we screened a range of power values and found that a power value equal to 14 resulted in high degrees of independence and average connectivity (**Additional Figure 1**). When this power value was used to generate the weighted co-expression network model, the 13,331 genes identified in the proximal segment were divided into 31 modules (**Figure 1A**). We next applied a Pearson correlation algorithm to calculate the correlation coefficient and P values of representative module genes and time to determine the importance of each proximal module (**Figure 1B**). In parallel, the 10,726 genes of distal segment were divided into 15 modules (**Figure 2A**), and the relative significance of the 15 modules was also determined based on Pearson correlation analysis (**Figure 2B**). The genes included in each module are listed in **Additional Table 2**. The significant modules for both the proximal and distal segments are shown in **Figures 1B** and **2B**.

Functional enrichment analysis of genes in modules that correlate significantly with time

As described above, we used WGCNA to identify significant gene co-expression modules in proximal and distal nerve stumps from rats after sciatic nerve injury. Next, we performed KEGG and GO functional analyses of genes in selected modules to further understand the functional differences and similarities between the proximal and distal modules. There were significant differences in the KEGG pathways and biology processes that were enriched in the proximal and distal modules. The red proximal module was mainly enriched in genes related to axon guidance, extracellular matrix-receptor interaction, cell adhesion, and cyclic adenosine monophosphate signaling (**Figure 3A**), while the purple and blue proximal modules were mainly enriched in genes related to lysosomes, the cell cycle, DNA replication, and cytokine-cytokine interactions (**Figure 3B** and **C**). Most of these pathways have been previously reported to be involved in nerve regeneration. The distal modules were primarily enriched in genes involved in degeneration-related pathways such as calcium signaling, lysosomes, glycan degeneration, and fatty acid degeneration (**Figure 3D–F**). Consistent with this, GO enrichment analysis showed that the proximal modules were enriched in genes involved to nerve regeneration–related processes, and distal modules were enriched in genes related to nerve degeneration (**Additional Figure 2**).

To our surprise, genes related to inflammation, which is triggered by axonal degeneration distal to nerve damage and is an essential part of WD (Dubový et al., 2013), were enriched in the proximal modules instead of the distal modules that correlated positively with time (**Figure 3C** and **Additional Figure 2A**). To further investigate this apparent contradiction, we analyzed other modules. GO annotation analysis identified two modules that were associated with inflammation in distal segments (**Additional Figure 3A** and **B**). These two modules were positively correlated with time only 1 to 24 hours after injury, and were negatively correlated or uncorrelated with time until 14 days post-injury (**Figure 2B**). Many biological process categories, such as the inflammatory response, the immune response, wound healing, and cytokine-mediated signaling, were enriched in the two distal modules (**Additional Figure 3A** and **B**). These enriched categories are important for the onset of WD. These results are consistent with a previous study that suggested that there are three distinct phases within the 4-week post-injury period. The first two phases include 0 to 6 hours post-injury, which involves the acute response to injury, and 6 to 24 hours post-injury, which is associated with WD. The extended up-regulation of the inflammatory response observed in the blue proximal module may be associated with the induction of neuropathic pain following nerve injury. Some of the genes included in this module were previously reported to be related to neuropathic pain, such as *Cxcl13*, *Ccl2*, and *Cxcr3*. Thus, it appears that inflammation after nerve injury is important not only for promoting nerve regeneration, but also for improving functional recovery.

Next, we performed functional enrichment analysis of genes in the proximal and distal modules that were negatively correlated with time (**Figure 4** and **Additional Figure 4**). As shown in **Figure 4A–C**, the three proximal modules were primarily enriched in genes involved in metabolism-related pathways such as fatty acid elongation, unsaturated fatty acid biosynthesis, and nitrogen metabolism. Axon regeneration after injury requires a large supply of energy, so these functions, as well as those of other metabolic pathways that store or consume large amounts of energy, may be down-regulated to help the damaged neurons successfully regenerate without undergoing an energy crisis. Two distal segment modules were also enriched in genes related to metabolism (**Figure 4D** and **E**). The relevant KEGG pathways are listed in **Additional Tables 3** and **4**. Another distal

module, the purple module, was enriched in genes involved in inflammatory- and apoptosis-related signaling pathways, which is consistent with the results from the GO enrichment analysis described above (**Figure 4F**). As discussed above, although genes in the purple distal module were negatively correlated with time overall, they were up-regulated at 1 and 6 hours post-injury, presumably due to participation in the initiation of WD. Furthermore, several biological processes were enriched in both proximal and distal modules (**Additional Figure 5**). In brief, processes associated with response to injury such as wound healing and drug response were up-regulated in both proximal and distal segments (**Additional Figure 5A**), while processes associated with energy-storing metabolic processes such as cholesterol and sterol biosynthesis were down-regulated in both segments over time (**Additional Figure 5B**). Taken together, our results suggest that peripheral nerve repair is a dynamic process that requires analysis at different time points, and that WGCNA can provide comprehensive insight into this process.

Identification of key genes related to axon regeneration and wallerian degeneration

To identify key genes regulating axon regeneration and WD, we selected the blue proximal module and the turquoise distal module for further analysis. In total, 544 and 264 critical genes that were positively associated with time were identified in the blue proximal module and the turquoise distal module, respectively, based on an MM threshold of > 0.9 and a GS threshold of > 0.5 (**Figure 5A** and **B** and **Additional Table 5**). Next, Cytoscape software was used to calculate intramodular connectivity within each of the two modules and identify the 50 genes in each module with the greatest degree of intramodular connectivity, which we designated as hub genes (**Figure 5C** and **D**). Interestingly, we found that *Ngfr* and *Kif22* were not only critical genes associated with time (**Additional Table 5**), but were also hub genes in both the blue proximal module and the turquoise distal module (**Figure 5C** and **D**). Ngfr, or nerve growth factor receptor, has been previously shown to be up-regulated in SCs after nerve injury, and to interact synergistically with nerve growth factor to guide axon regeneration and activate autophagy in SCs to enhance myelin debris clearance during WD, thus playing important role in peripheral nerve repair (Zhou and Li, 2007; Webber et al., 2008; Jessen and Mirsky, 2016; Li et al., 2020b). *Kif22* is a microtubule positive-end tracking protein that is crucial for cell mitosis, centrosome separation, and spindle formation (Yu et al., 2020). Previous studies have shown that *Kif22* promotes cancer cell proliferation and metastasis (Yu et al., 2014, 2020). However, the role of *Kif22* in peripheral nerve repair is currently unknown. To verify the microarray and WGCNA results for *Kif22*, we performed quantitative real-time polymerase chain reaction and found that *Kif22* mRNA expression was significantly up-regulated from 4 days post-nerve injury in both the proximal and distal nerve stumps (**Figures 1A**, **5E** and **5F**), indicating a potential role for *Kif22* in axon regeneration and WD. Collectively, these results suggest that *Kif22* activity is an important part of peripheral nerve repair.

***Kif22* regulates SC proliferation and migration via PKCα-mediated ERK signaling**

SCs, which are the most important glial cells in the peripheral nervous system, play an essential role in peripheral nerve development and function, and especially in peripheral nerve repair after injury. After injury, myelinating and non-myelinating (Remak) SCs de-differentiate, activate, or reprogram to convert into repair SCs (Jessen and Mirsky, 2016). Then, the repair SCs further proliferate, migrate, form bands of Büngner to guide axon regeneration, and secrete a variety of cytokines and neurotrophic factors to activate macrophages to engulf myelin fragments, thereby initiating WD and promoting nerve regeneration (Jessen and Mirsky, 2016; Jessen and Arthur-Farraj, 2019). Given the role of SCs in axon regeneration and WD and the critical role of *Kif22* in regulating cancer cell proliferation and metastasis, we next asked whether the effect of *Kif22* on SC proliferation and migration promotes peripheral nerve repair. First, we designed three *Kif22*-specific siRNAs to knock down *Kif22* expression in SCs. As shown in **Figure 5A**, all three *Kif22*-specific siRNAs significantly reduced *Kif22* expression. We used the two most effective *Kif22*-specific siRNAs to silence *Kif22* in SCs and investigate the effect of *Kif22* knockdown on SC proliferation and migration. An EdU assay showed that *Kif22* knockdown decreased the rate of SC proliferation (**Figure 6B** and **C**), and a Transwell assay showed that *Kif22* knockdown disrupted SC migration (**Figure 6D** and **E**). The wound healing assay further validated the negative effect of *Kif22* knockdown on SC migration (**Figure 6F** and **G**). Taken together, these results suggest that *Kif22* promotes SC proliferation and migration.

We next explored the mechanisms underlying *Kif22*-mediated regulation of SC proliferation and migration. We first analyzed the effects of *Kif22* knockdown on the expression of genes involved in cell cycle and migration. In general, *Kif22* knockdown stably decreased the expression of several genes involved in the cell cycle, including cyclin dependent kinase 2 and cyclin D1 (**Figure 7A**). Cyclin D1 was identified as a critical gene associated with time in both the blue proximal module and the turquoise distal module based on an MM threshold of > 0.9 and a GS threshold of > 0.5 (**Additional Table 5**). Consistent with this finding, cyclin D1 has been previously reported to be down-regulated by *Kif22* silencing, thereby inhibiting the proliferation of gastric cancer cells (Yu et al., 2020). These findings strongly suggest that *Kif22* knockdown can drastically decreased the expression of cyclin dependent kinase 2 and cyclin D1 to disrupt SC proliferation. *Kif22* knockdown also significantly reduced the expression of genes involved in cell migration, such as vimentin and cadherin 2 (**Figure 7B**). These two genes encode key adhesion molecules that regulate SC migration (Clements et al., 2017; Yao et al., 2020). Therefore, our findings suggest that *Kif22* knockdown inhibits SC migration by modulating the expression of vimentin and cadherin 2.

Next, we explored the mechanism by which *Kif22* contributes to altering the expression of genes related to the cell cycle and migration. The ERK signaling pathway plays an important role in SC proliferation and migration, as well as regulation of axon regeneration and WD (Napoli et al., 2012; Li et al., 2020a). The ERK signaling pathway is regulated by numerous upstream signals, including epidermal growth factor, insulin-like growth factor, and other growth factor signals, as well as PKCα (Yin et al., 2013; Sun et al., 2015). A previous study found that PKCα is up-regulated in rat SCs from distal sciatic nerve stumps after injury and activates the ERK signaling pathway to promote SC proliferation and migration (Li et al., 2020a). However, here we found that PKCα was down-regulated by *Kif22* knockdown in SCs (**Figure 7C–E**). Moreover, a previous study reported that *Kif22* is related to the ERK signaling pathway, and that *Kif22* knockdown reduces p-ERK expression levels in gastric cancer cells (Yu et al., 2020). Thus, we asked whether altering *Kif22* expression would affect activation of the ERK signaling pathway in SCs. Western blot analysis showed that knocking down *Kif22* in SCs with *Kif22*-specific siRNAs significantly inhibited ERK phosphorylation (**Figure 7D** and **E**). Taken together, these date indicate that *Kif22* modulates SC proliferation and migration by affecting PKCα expression and thereby activating the ERK signaling pathway.

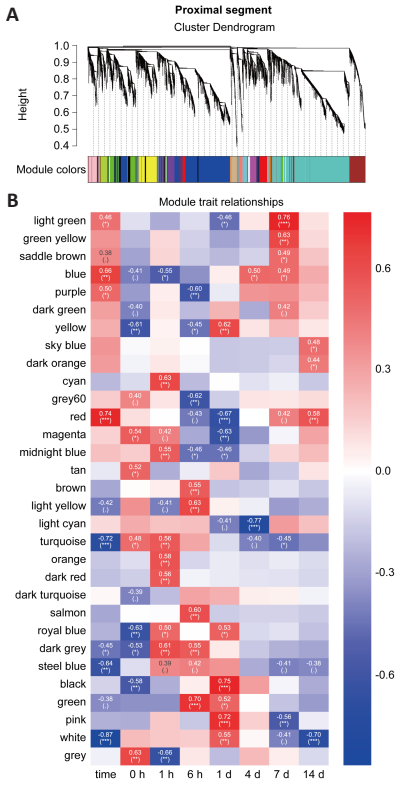

Figure 1 | WGCNA and identification of significant DEG modules from proximal nerve segments.
(A) Clustering dendrogram (upper part) and distribution (lower part) of the genes in each module. The different colors indicate 31 different modules. The wider the colored bar, the more genes the module contains. (B) Heatmap of correlation analysis of the modules and trait at different time points post-nerve injury. The correlation coefficient between the modules and total time is shown in the far left column of the heatmap. *P* values are shown for the indicated modules. $*P < 0.05$, $**P < 0.01$, $***P < 0.001$. DEG: Differentially expressed gene; WGCNA: weighted gene co-expression network analysis.

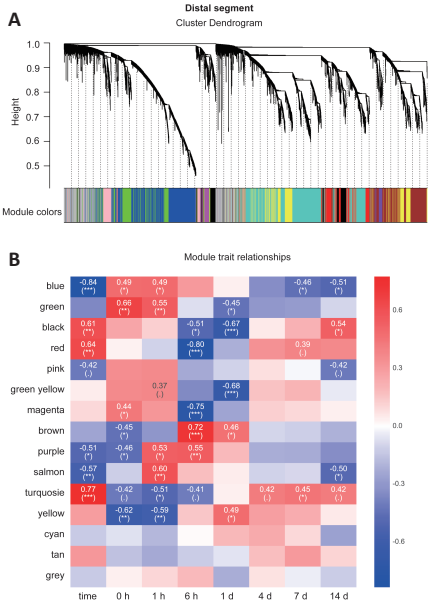

Figure 2 | WGCNA and identification of significant DEG modules from distal nerve segments.
(A) Clustering dendrogram (upper part) and distribution (lower part) of the genes in each module. The different colors indicate the 15 different modules. (B) Heatmap of correlation analysis of the modules and trait at different time points post-nerve injury. The correlation coefficient between the modules and total time is shown in the far left column of the heatmap. *P* values are shown for the indicated modules. $*P < 0.05$, $**P < 0.01$, $***P < 0.001$. DEG: Differentially expressed gene; WGCNA: weighted gene co-expression network analysis.

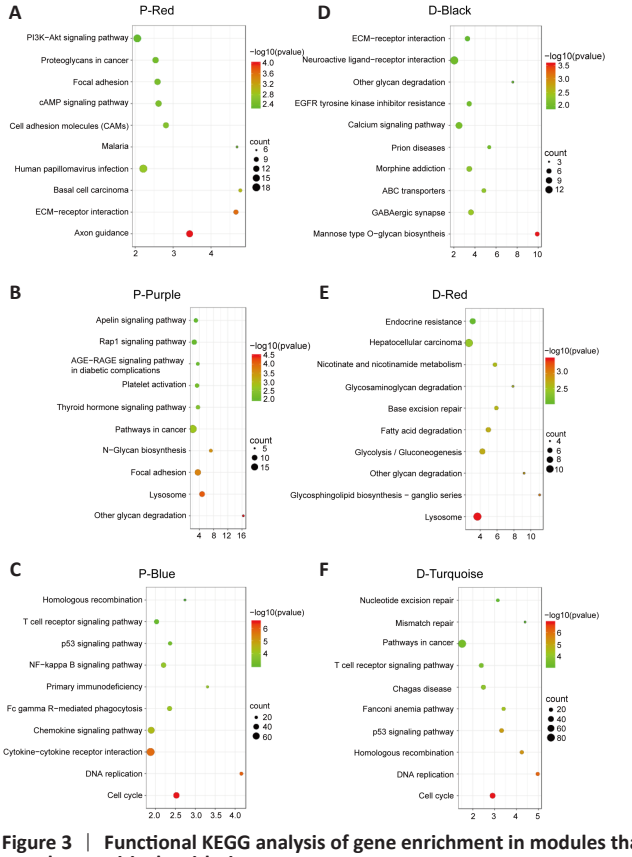

Figure 3 | Functional KEGG analysis of gene enrichment in modules that correlate positively with time.
(A–C) KEGG plots of the genes in the three proximal modules (red, purple, and blue) that correlated positively with time. The *P* value of the purple module was 0.5. (D–F) KEGG plots of the genes in the three distal modules (black, red, and turquoise) that correlated positively with time. The horizontal axis shows the enrichment score, and the vertical axis shows the functional description of the enriched pathway. The larger the circle, the more genes were associated with this function. The color spectrum from green to red represents the uncorrected *P* value. KEGG: Kyoto Encyclopedia of Genes and Genomes.

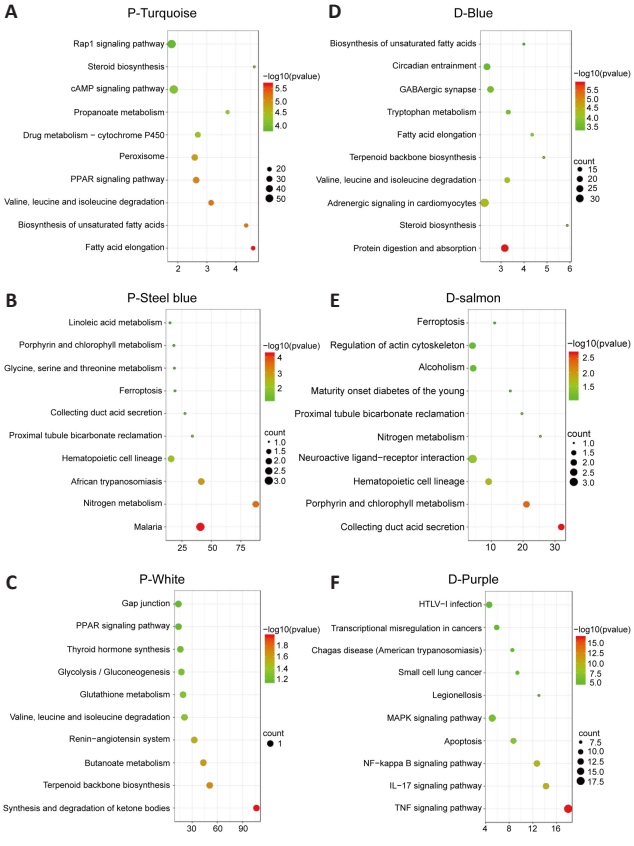

Figure 4 | Functional KEGG analysis of genes enriched in modules that correlate negatively with time.
(A–C) KEGG plots of genes in the three proximal modules (turquoise, steel blue, and white) that correlated negatively with time. (D–F) KEGG plots of genes in three distal modules (blue, salmon and purple) that correlated negatively with time. The horizontal axis shows the enrichment score, and the vertical axis shows the functional description of the enriched pathway. The larger the circle, the more genes were associated with this function. The color spectrum from green to red represents the uncorrected *P* value. KEGG: Kyoto Encyclopedia of Genes and Genomes.

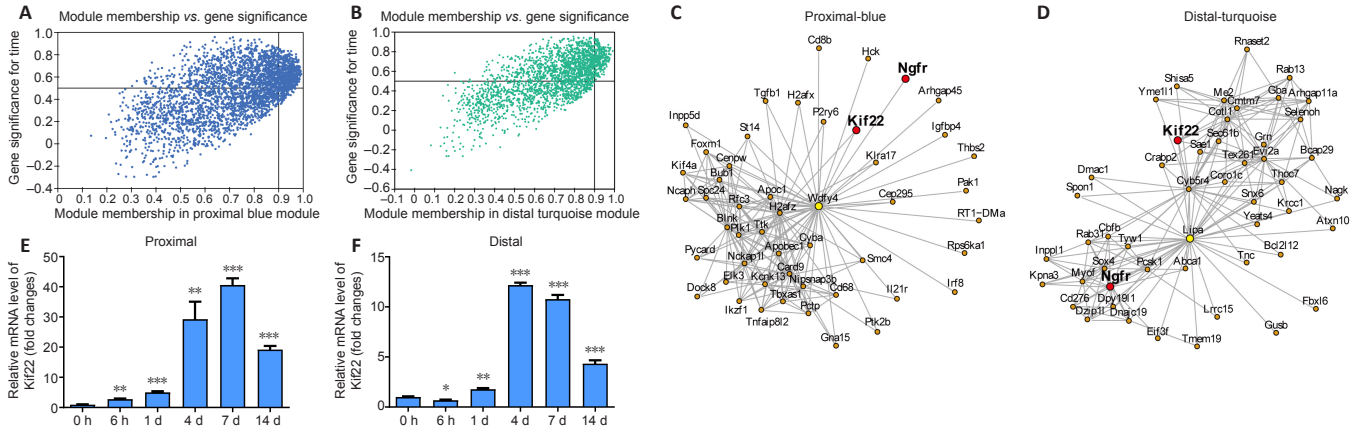

Figure 5 | **Kinesin family member 22 (*Kif22*) is the key hub gene that correlates positively with time in both the proximal and distal segments.**
(A, B) Scatter plot of gene significance (GS) *vs*. module membership (MM) in the blue proximal module (A) or the turquoise distal module (B). The key genes were identified based on the following thresholds: MM > 0.9 and GS > 0.5. (C, D) Hub gene network in the blue proximal module (C) and the turquoise distal module (D). The central key gene in each hub gene network is highlighted in yellow. The genes that were differentially expressed in both the blue proximal module and the turquoise distal module are highlighted in red. (E, F) *Kif22* mRNA expression in proximal and distal nerve stumps from rats at different time points after nerve transection surgery. All data are shown as mean ± SD (n = 3). *P < 0.05, **P < 0.01, ***P < 0.001, *vs*. 0-h group (unpaired t-test).

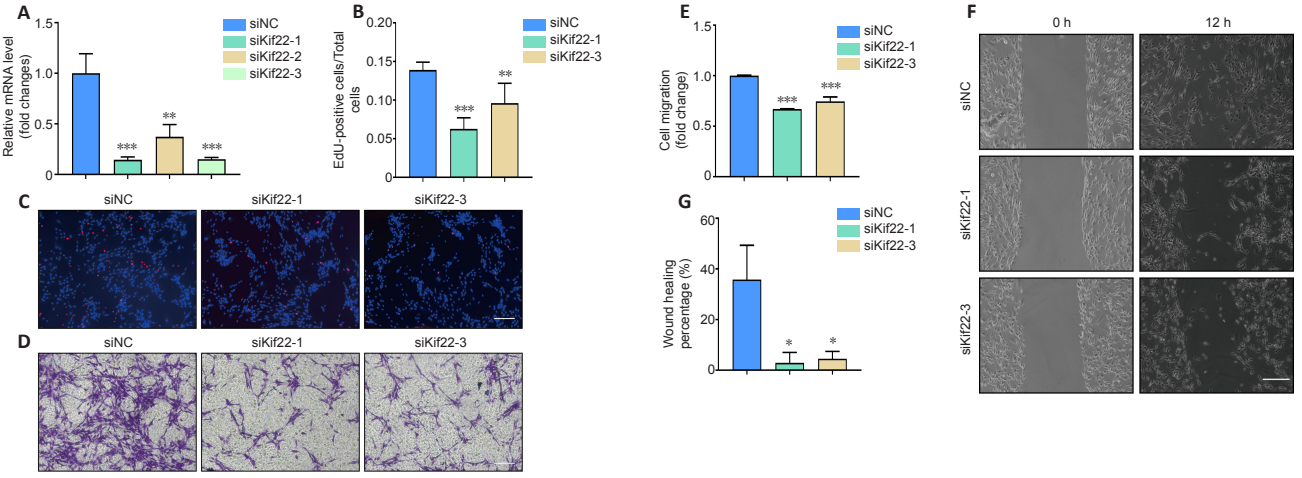

Figure 6 | **The effect of *Kif22* knockdown on SC proliferation and migration.**
(A) *Kif22* mRNA expression in SCs transfected with negative control siRNA (siNC) or *Kif22*-specific siRNA (siKif22-1–3). (B, C) Effect of *Kif22* knockdown on SC proliferation. (B) Quantitation of EdU-positive cells. (C) The cells were stained with EdU (red), and the nucleus was stained with Hoechst 33342 (blue). SCs transfected with siKif22s showed a significant decrease in EdU-positivity compared with SCs transfected with siNC. (D–G) Effect of *Kif22* knockdown on SC migration. (D) Wound healing assay. There was no difference between the siKif22 group and the siNC group at 0 hours, while at later time points the siKif22 group showed a lower rate of wound healing than the siNC group (quantitation shown in E). (F) Transwell assay. The siKif22 group displayed a slower rate of cell migration than the siNC group (quantitation shown in G). Scale bars: 100 μm in C, D, F. All data are shown as mean ± SD. All experiments were repeated in triplicate. *P < 0.05, **P < 0.01, ***P < 0.001, *vs*. siNC group (unpaired t-test). EdU: 5-Ethynyl-2′-deoxyuridine; Kif22: kinesin family member 22; SC: Schwann cell; siRNA: small interfering RNA.

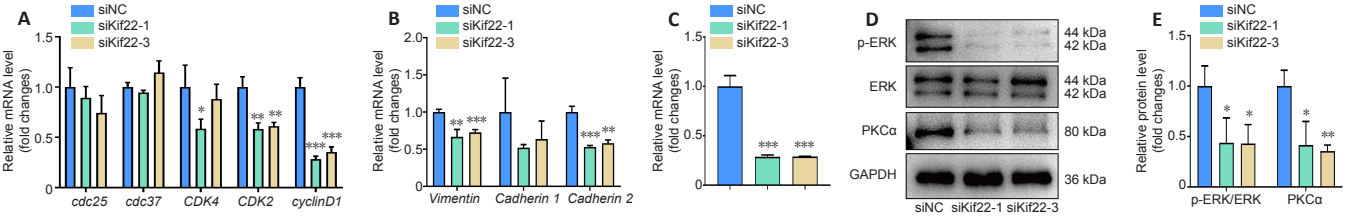

Figure 7 | **Kif22 knockdown decreases PKCα expression, resulting in inactivation of the ERK signaling pathway.**
(A, B) The mRNA expression level of genes related to cell proliferation or migration in SCs transfected with negative control siRNA (siNC) or Kif22-specific siRNA (siKif22-1 or -3). (C) The effect of *Kif22* knockdown on *PKCα* mRNA expression. (D) The effect of *Kif22* knockdown on activation of the ERK signaling pathway. (E) Quantification of protein expression levels. All data are shown as mean ± SD. All experiments were repeated in triplicate. *P < 0.05, **P < 0.01, ***P < 0.001, *vs*. siNC group (unpaired t-test). ERK: Mitogen-activated protein kinase 1; GAPDH: glyceraldehyde-3-phosphate dehydrogenase; Kif22: kinesin family member 22; PKCα: protein kinase C α; SC: Schwann cell; siRNA: small interfering RNA.

Discussion

Peripheral nerve injury repair is a complex process that is dependent on effective WD and, subsequently, successful axon regeneration. In this study, we applied WGCNA to systematically analyze the transcriptomes of proximal and distal nerve stumps from rats subjected to sciatic nerve injury, with the aim of better understanding the cellular and molecular mechanisms that underlie the coordinated regulation of axon regeneration and WD in peripheral nerve injury repair.

Using WGCNA, we identified 31 and 15 co-expression modules in proximal and distal nerve segments, respectively, from rats with sciatic nerve injury. We then selected the most significant co-expression modules and performed KEGG and GO enrichment analyses of the genes in these modules to further understand the functional differences and similarities between the two segments. The results from these analyses showed that nerve regeneration-related biological processes were up-regulated in proximal modules, whereas nerve degeneration-related biological processes were up-regulated in distal modules. Genes associated with inflammation were enriched in both the proximal and distal modules. However, the inflammation-related genes in the proximal modules were positively correlated with time, while those in the distal modules were negatively correlated with time, and were first up-regulated and then down-regulated. This may reflect an important difference between the mechanisms involved in axon regeneration and WD. In addition, the proximal and distal modules showed some similarities in terms of enriched biological processes, including up-regulation of genes involved in processes associated with response to injury such as wound healing and drug response, as well as downed-regulated processes associated with energy-storing metabolism such as cholesterol and sterol biosynthesis. Taken together, these findings suggest ways in which regeneration and degeneration could be targeted separately or together for therapeutic purposes.

In this study, we identified *Kif22* as a hub gene that is positively associated with time in both proximal and distal segments. *Kif22* is a member of the kinesin-like family of proteins, which are microtubule-dependent molecular motors with DNA-binding capacity (Yu et al., 2014). *Kif22* has been previously reported to promote cancer cell proliferation and migration (Yu et al., 2014, 2020; Pike et al., 2018). In addition, we found that *Kif22* knockdown substantially inhibits SC proliferation and migration, indicating a potential role for *Kif22* in axon regeneration and WD. Furthermore, *Kif22* knockdown reduced the expression of cell cycle- and migration-related genes, as well as the expression of PKCα. PKCα is a positive regulator of the ERK signaling pathway, which promotes SC proliferation and migration (Li et al., 2020a). Consistent with this, reduced expression of PKCα in *Kif22*-knockdown SCs led to delayed activation of the ERK signaling pathway. Though *Kif22* has been previously reported to affect ERK activation, the mechanism underlying *Kif22*-mediated regulation of the ERK signaling pathway has not yet been determined (Yu et al., 2020). The findings from our study suggest that *Kif22* regulates the ERK signaling pathway by modulating PKCα expression. However, the molecular mechanism by which *Kif22* regulates PKCα expression remains unclear. *Kif22* was previously shown to not only act as a motor protein during cell mitosis, but also transcriptionally regulate cancer development (Yu et al., 2014). Thus, we speculate that *Kif22* regulates PKCα transcription, which should be explored in future studies. Collectively, these data suggest a new role for *Kif22* in peripheral nerve injury repair and a new mechanism by which *Kif22* regulates the ERK signaling pathway.

The current study suggests that *Kif22* mechanistically regulates nerve repair by modulating ERK signaling-mediated SC proliferation and migration. However, as an important regulator of cell division, proliferation, and migration, *Kif22* may not only act on nonnneuronal cell proliferation but also be repurposed from its mitotic role to play a cytoplasmic role in neurons. *Kif22* is a motor protein that can regulate microtubule dynamics to delay epidermal growth factor receptor internalization and enhance epidermal growth factor receptor signaling (Pike et al., 2018), and the findings from our study suggest that it may also regulate the transport of growth factors to regulate nerve regeneration. Microtubules, as an important part of the cytoskeleton, play essential roles in nerve regeneration (He et al., 2016; Blanquie and Bradke, 2018); thus, *Kif22* may regulate microtubule dynamics to participate in nerve repair. Future studies should explore these possible molecular mechanisms underlying *Kif22*-modulated nerve repair.

In summary, this study provides a comprehensive comparison of proximal axon regeneration and distal axon WD. We found that *Kif22* is a positive regulator of SC proliferation and migration, processes that are essential in axon regeneration and WD, highlighting potential new therapeutic targets for treating peripheral nerve injury. However, while we verified that *Kif22* mechanistically regulates nerve repair by modulating ERK signaling-mediated proliferation and migration of SCs, it remains unclear whether the role of *Kif22* in mitosis, microtubule dynamics, or transport of growth factors is also a part of this process. In addition, we only focused on hub genes with the same expression pattern in both proximal and distal segments, so hub genes with different expression patterns in these segments merit further study.

Author contributions: *Study conceptualization: QQC, BY; study design, data analysis and manuscript writing: QQC; experiment implementation: YL, QS; technical assistance: ML, XAN; English writing assistance and manuscript review: SSM. All authors read and approved the final version of the manuscript.*
Conflicts of interest: *The authors declare no conflict of interest.*
Financial support: *This study was supported by the National Major Project of Research and Development of China, No. 2017YFA0104701 (to BY); the National Natural Science Foundation of China, No. 32000725 (to QQC); the Natural Science Foundation of Jiangsu Province of China, No. BK20200973 (to QQC); and the Jiangsu Provincial University Innovation Training Key Project of China, No. 202010304021Z (to ML). The funders had no role in study design, data collection and analysis, decision to publish, or preparation of the manuscript.*
Institutional review board statement: *This study was approved by the Institutional Animal Care guidelines of Nantong University, China (approval No. S20210322-008) on March 22, 2021.*

Data sharing statement: *Datasets analyzed during the current study are available from the corresponding author on reasonable request.*
Plagiarism check: *Checked twice by iThenticate.*
Peer review: *Externally peer reviewed.*

Additional files:
Additional Table 1: *List of primers used in quantitative real-time polymerase chain reaction.*
Additional Table 2: *The number of genes in different modules of proximal and distal nerve segments of rats with sciatic nerve injury during Wallerian degeneration.*

Additional Table 3: *The list of enriched KEGG pathway related to Figure 3.*
Additional Table 4: *The list of enriched KEGG pathway related to Figure 4.*
Additional Table 5: *List of moddule membership and gene significance in proximal blue and distal turquoise modules.*
Additional Figure 1: *Analysis of network topology for various soft-thresholding powers.*
Additional Figure 2: *Functional GO enrichment of genes in modules that positively correlated with time.*
Additional Figure 3: *Functional enrichment of genes in modules that first positively .then negatively correlated with time.*
Additional Figure 4: *Functional enrichment of genes in modules that negatively correlated with time.*
Additional Figure 5: *The overlap between the biological function of proximal and distal segments.*

References

Blanquie O, Bradke F (2018) Cytoskeleton dynamics in axon regeneration. Curr Opin Neurobiol 51:60-69.

Clements MP, Byrne E, Camarillo Guerrero LF, Cattin AL, Zakka L, Ashraf A, Burden JJ, Khadayate S, Lloyd AC, Marguerat S, Parrinello S (2017) The wound microenvironment reprograms Schwann cells to invasive mesenchymal-like cells to drive peripheral nerve regeneration. Neuron 96:98-114.e7.

Coleman MP, Freeman MR (2010) Wallerian degeneration, wld(s), and nmnat. Annu Rev Neurosci 33:245-267.

Conforti L, Gilley J, Coleman MP (2014) Wallerian degeneration: an emerging axon death pathway linking injury and disease. Nat Rev Neurosci 15:394-409.

Dubový P, Jančálek R, Kubek T (2013) Role of inflammation and cytokines in peripheral nerve regeneration. Int Rev Neurobiol 108:173-206.

Girouard MP, Bueno M, Julian V, Drake S, Byrne AB, Fournier AE (2018) The molecular interplay between axon degeneration and regeneration. Dev Neurobiol 78:978-990.

He M, Ding Y, Chu C, Tang J, Xiao Q, Luo ZG (2016) Autophagy induction stabilizes microtubules and promotes axon regeneration after spinal cord injury. Proc Natl Acad Sci U S A 113:11324-11329.

He Z, Jin Y (2016) Intrinsic control of axon regeneration. Neuron 90:437-451.

Jessen KR, Mirsky R (2016) The repair Schwann cell and its function in regenerating nerves. J Physiol 594:3521-3531.

Jessen KR, Arthur-Farraj P (2019) Repair Schwann cell update: Adaptive reprogramming, EMT, and stemness in regenerating nerves. Glia 67:421-437.

Jiang N, Li H, Sun Y, Yin D, Zhao Q, Cui S, Yao D (2014) Differential gene expression in proximal and distal nerve segments of rats with sciatic nerve injury during Wallerian degeneration. Neural Regen Res 9:1186-1194.

Li J, Zhang Z, Wang J, Du S, Yao D, Cao R, Cui S (2020a) Protein kinase Cα promotes proliferation and migration of Schwann cells by activating ERK signaling pathway. Neuroscience 433:94-107.

Li R, Li D, Wu C, Ye L, Wu Y, Yuan Y, Yang S, Xie L, Mao Y, Jiang T, Li Y, Wang J, Zhang H, Li X, Xiao J (2020b) Nerve growth factor activates autophagy in Schwann cells to enhance myelin debris clearance and to expedite nerve regeneration. Theranostics 10:1649-1677.

Liu X, Hu AX, Zhao JL, Chen FL (2017) Identification of key gene modules in human osteosarcoma by co-expression analysis weighted gene co-expression network analysis (WGCNA). J Cell Biochem 118:3953-3959.

Mahar M, Cavalli V (2018) Intrinsic mechanisms of neuronal axon regeneration. Nat Rev Neurosci 19:323-337.

Napoli I, Noon LA, Ribeiro S, Kerai AP, Parrinello S, Rosenberg LH, Collins MJ, Harrisingh MC, White IJ, Woodhoo A, Lloyd AC (2012) A central role for the ERK-signaling pathway in controlling Schwann cell plasticity and peripheral nerve regeneration in vivo. Neuron 73:729-742.

Pike R, Ortiz-Zapater E, Lumicisi B, Santis G, Parsons M (2018) KIF22 coordinates CAR and EGFR dynamics to promote cancer cell proliferation. Sci Signal 11:eaaq1060.

Prior R, Van Helleputte L, Benoy V, Van Den Bosch L (2017) Defective axonal transport: a common pathological mechanism in inherited and acquired peripheral neuropathies. Neurobiol Dis 105:300-320.

Smith GM, Gallo G (2018) The role of mitochondria in axon development and regeneration. Dev Neurobiol 78:221-237.

Sun Y, Liu WZ, Liu T, Feng X, Yang N, Zhou HF (2015) Signaling pathway of MAPK/ERK in cell proliferation, differentiation, migration, senescence and apoptosis. J Recept Signal Transduct Res 35:600-604.

Wan Q, Tang J, Han Y, Wang D (2018) Co-expression modules construction by WGCNA and identify potential prognostic markers of uveal melanoma. Exp Eye Res 166:13-20.

Webber CA, Xu Y, Vanneste KJ, Martinez JA, Verge VM, Zochodne DW (2008) Guiding adult mammalian sensory axons during regeneration. J Neuropathol Exp Neurol 67:212-222.

Yao C, Chen Y, Wang J, Qian T, Feng W, Chen Y, Mao S, Yu B (2020) LncRNA BC088259 promotes Schwann cell migration through Vimentin following peripheral nerve injury. Glia 68:670-679.

Yao C, Shi X, Zhang Z, Zhou S, Qian T, Wang Y, Ding F, Gu X, Yu B (2016) Hypoxia-induced upregulation of miR-132 promotes schwann cell migration after sciatic nerve injury by targeting PRKAG3. Mol Neurobiol 53:5129-5139.

Yao D, Li M, Shen D, Ding F, Lu S, Zhao Q, Gu X (2013) Expression changes and bioinformatic analysis of Wallerian degeneration after sciatic nerve injury in rat. Neurosci Bull 29:321-332.

Yi S, Tang X, Yu J, Liu J, Ding F, Gu X (2017) Microarray and qPCR analyses of wallerian degeneration in rat sciatic nerves. Front Cell Neurosci 11:22.

Yin Y, Sun W, Li Z, Zhang B, Cui H, Deng L, Xie P, Xiang J, Zou J (2013) Effects of combining methylprednisolone with rolipram on functional recovery in adult rats following spinal cord injury. Neurochem Int 62:903-912.

Yu J, Gu X, Yi S (2016) Ingenuity pathway analysis of gene expression profiles in distal nerve stump following nerve injury: insights into Wallerian degeneration. Front Cell Neurosci 10:274.

Yu Y, Wang XY, Sun L, Wang YL, Wan YF, Li XQ, Feng YM (2014) Inhibition of KIF22 suppresses cancer cell proliferation by delaying mitotic exit through upregulating CDC25C expression. Carcinogenesis 35:1416-1425.

Yu ZY, Jiang XY, Zhao RR, Qin JJ, Luo CJ, Ren YX, Ren W, Ma ZJ, Jiao ZY (2020) Effect of KIF22 on promoting proliferation and migration of gastric cancer cells via MAPK-ERK pathways. Chin Med J (Engl) 133:919-928.

Zhang B, Horvath S (2005) A general framework for weighted gene co-expression network analysis. Stat Appl Genet Mol Biol 4:Article17.

Zhou XF, Li HY (2007) Roles of glial p75NTR in axonal regeneration. J Neurosci Res 85:1601-1605.

C-Editor: Zhao M; S-Editors: Yu J, Li CH; L-Editors: Crow E, Yu J, Song LP; T-Editor: Jia Y

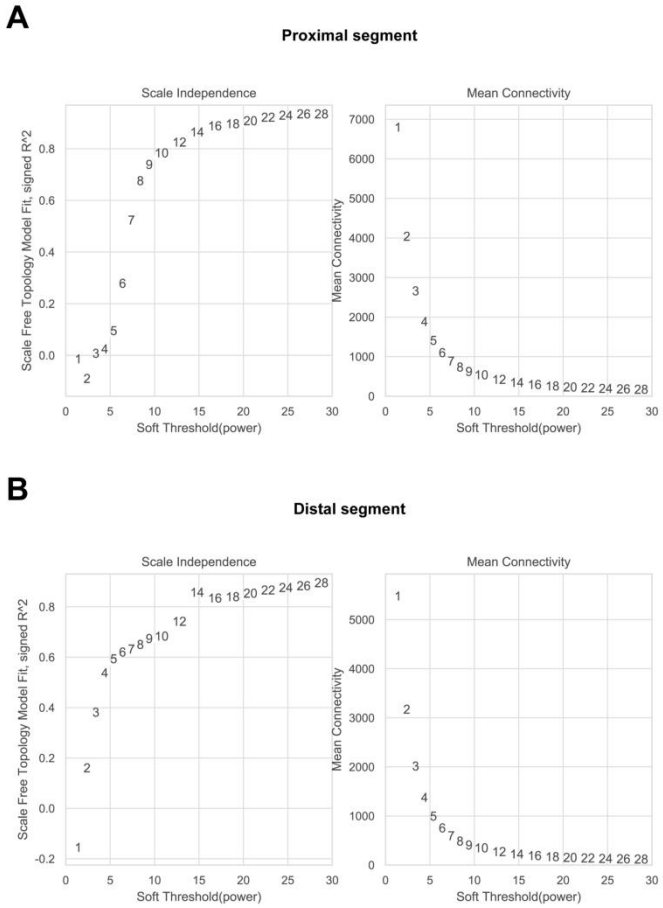

Additional Figure 1 Analysis of network topology for various soft-thresholding powers.

(A, B) Filter results for power values of proximal (A) and distal (B) networks. The figure on the left is the correlation coefficient corresponding to different power values, and the figure on the right is the average connectivity degree of the network constructed by different power values.

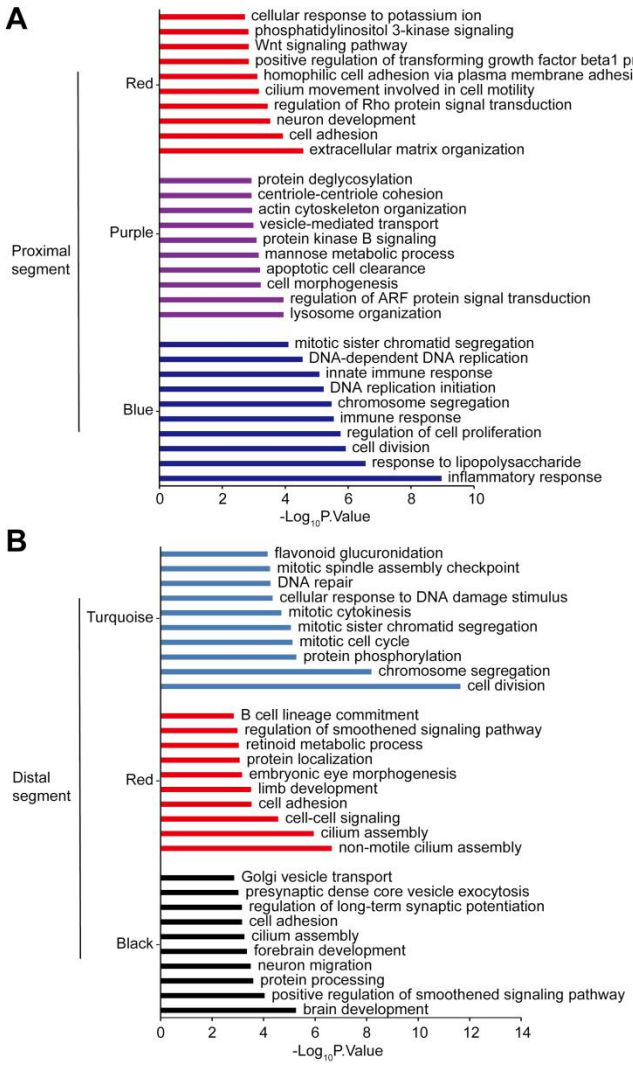

Additional Figure 2 Functional GO enrichment of genes in modules that positively correlated with time.
(A) GO enrichment analysis of genes in three proximal modules (red, purple and blue modules) that positively correlated with time. Among them P value of purple module was 0.5. (B) GO enrichment analysis of genes in three distal modules (turquoise, red and black modules) that positively correlated with time. The horizontal axis represents the $\log_{10}$P value of the significant GO terms. The vertical axis represents different modules. GO: Gene ontology.

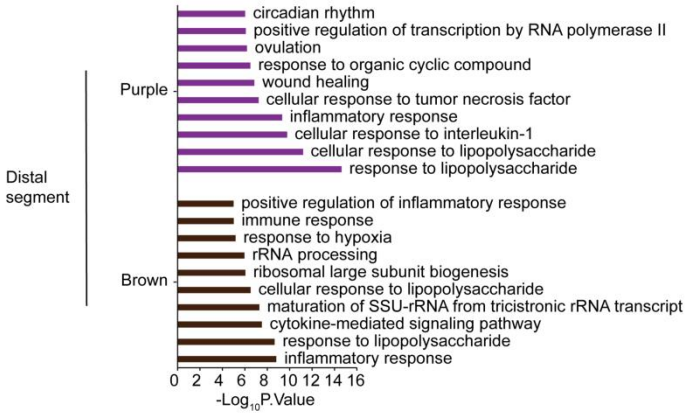

Additional Figure 3 Functional enrichment of genes in modules that first positively then negatively correlated with time.

GO enrichment analysis of genes in purple and brown modules of distal segment. The horizontal axis represents the $\log_{10}$P value of the significant GO terms. The vertical axis represents different modules. GO: Gene ontology.

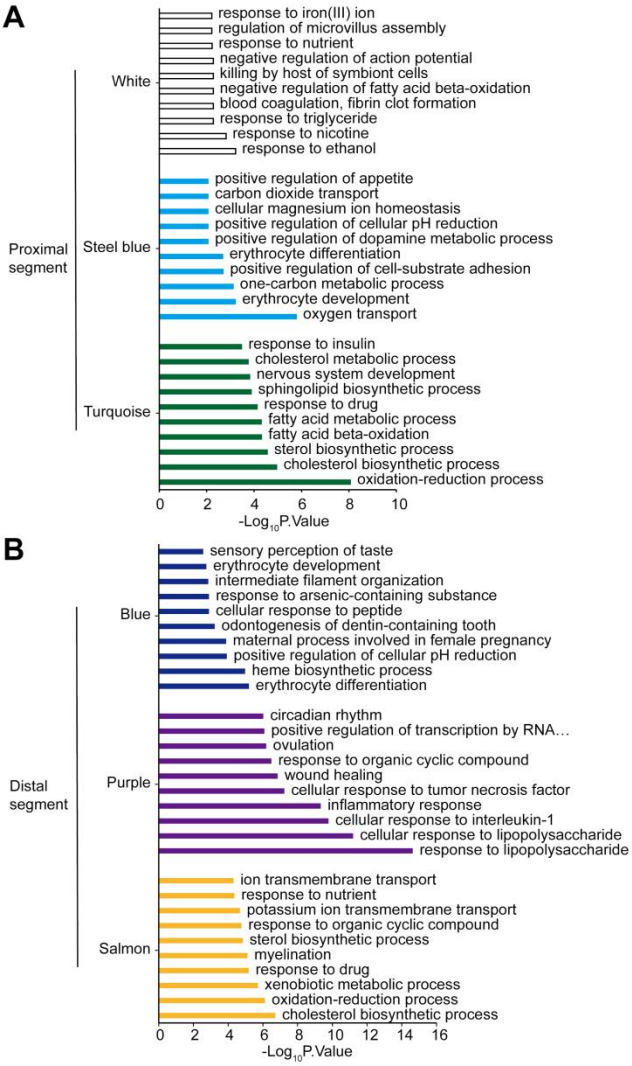

Additional Figure 4 Functional enrichment of genes in modules that negatively correlated with time.
(A) GO enrichment analysis of genes in three proximal modules that negatively correlated with time. (B) GO enrichment analysis of genes in three distal modules that negatively correlated with time. The horizontal axis represents the $\log_{10}$P value of the significant GO terms. The vertical axis represents different modules. GO: Gene ontology.

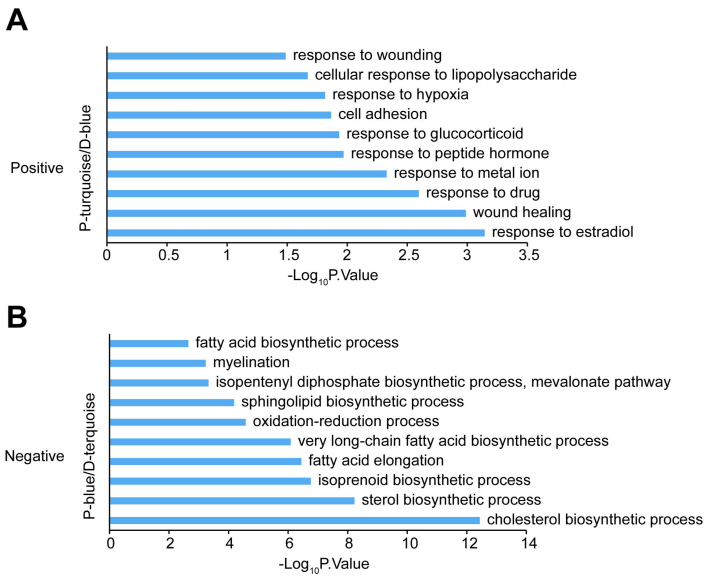

Additional Figure 5 The overlap between the biological function of proximal and distal segments.

(A) The common biological functions between proximal turquoise (P-turquoise) and distal blue (D-blue), whose genes are positively correlated with time. (B) The common biological functions between proximal blue (P-blue) and distal turquoise (D-turquoise), whose genes are negatively correlated with time. The horizontal axis represents the $\log_{10}$P value of the significant Gene ontology terms. The vertical axis represents different modules. GO: Gene ontology.

Additional Table 1 List of primers used in quantitative real-time polymerase chain reaction

Gene ID	Gene full name	Gene symbol	Primer sequences (5'-3')
293502	Kinesin family member 22	*Kif22*	Forward: TGC CAA CAT CGC TCC TGA AA Reverse: TTA ACA GGT GCC AAG GCA TGA
171102	Cell division cycle 25A	*Cdc25a*	Forward: ATG GGC TCC TCT GAA TCG AC Reverse: CCC CAA GAG CTT CTG AGG TA
114562	Cell division cycle 37	*Cdc37*	Forward: GGA GGA CAT GCG GCA AAA AG Reverse: GGT GGA GCA TGC CGA AAT GT
94201	Cyclin-dependent kinase 4	*CDK4*	Forward: GGA CCG ATC CCC GGT GTA Reverse: CGG AGC AGG GGA TCT TAC GC
362817	Cyclin-dependent kinase 2	*CDK2*	Forward: CTT TGC CGA AAT GGT GAC CC Reverse: TAA CTC CTG GCC AAA CCA CC
58919	Cyclin D1	*Cyclin D1*	Forward: TCA AGT GTG ACC CGG ACT G Reverse: CAC TAC TTG GTG ACT CCC GC
81818	Vimentin	*Vimentin*	Forward: TGC GGC TGC GAG AAA AAT TG Reverse: GGT CAA GAC GTG CCA GAG AA
83502	Cadherin 1	*Cadherin 1*	Forward: CCA GCG ACT GGT TCA GAT CA Reverse: GAT GAA AAC GCC AAC AGG GG
83501	Cadherin 2	*Cadherin 2*	Forward: CCT CCA ACG GGC ATC TTC AT Reverse: TCA TCA CAT ACG TCC CAG GC
24680	Protein kinase C, alpha	*PKCα*	Forward: GAA CAC ATG ATG GAC GGG GTC ACG AC Reverse: CGC TTG GCA GGG TGT TTG GTC ATA

Additional Table 2 The number of genes in different modules of proximal and distal nerve segments of rats with sciatic nerve injury during Wallerian degeneration

Module color	Frequency of genes
Proximal	
Black	475
Blue	3201
Brown	866
Cyan	200
Dark green	51
Dark grey	44
Dark orange	40
Dark red	53
Dark turquoise	50
Green	715
Green yellow	331
Light cyan	109
Light green	77
Light yellow	72
Magenta	372
Midnight blue	125
Orange	42
Pink	406
Purple	333
Red	645
Royal blue	66
Saddle brown	29
Salmon	201
Sky blue	30
Steel blue	28
Tan	272
Turquoise	3357
White	31
Yellow	841
Grey60	97
Grey	172
Total	13331
Distal	
Black	574
Blue	1944
Brown	1119
Cyan	22
Green	861
Green yellow	97
Magenta	204
Pink	323
Purple	148
Red	643
Salmon	47
Tan	59
Turquoise	2331
Yellow	1100

Grey	1254
Total	10726

Additional Table 4 The List of enriched KEGG pathway related to Figure 4

Term_ID	Term_description	ListHit	ListTotal	PopHit	PopTotal	FoldEnrichment	GeneIds	GeneSymbols	P_value	FDR_bh
P-Turquoise										
mmu00062	Fatty acid elongation	19	1211	28	8202	4.595906571	Hadh; Acot2; Acot4; Acaa2; Elovl6; Acot5; Hacd3; Echs1; Elovl7; Hacd2; Them4; Hacd4; Elovl4; Elovl1; Tecr; Acot1; Elovl5; Hsd17b12; Elovl3	Hadh; Acot2; Acot4; Acaa2; Elovl6; Acot5; Hacd3; Echs1; Elovl7; Hacd2; Them4; Hacd4; Elovl4; Elovl1; Tecr; Acot1; Elovl5; Hsd17b12; Elovl3	2.05565E-06	0.000633141
mmu01040	Biosynthesis of unsaturated fatty acids	18	1211	28	8202	4.354016751	Fads1; Acot2; Acot4; Elovl6; Fads2; Scd2; Hacd3; Acot5; Tecr; Hacd2; Hacd4; Acaa1b; Baat; Acaa1a; Acot1; Elovl5; Hsd17b12; Acox1	Fads1; Acot2; Acot4; Elovl6; Fads2; Scd2; Hacd3; Acot5; Tecr; Hacd2; Hacd4; Acaa1b; Baat; Acaa1a; Acot1; Elovl5; Hsd17b12; Acox1	6.6101E-06	0.000668716
mmu00280	Valine, leucine and isoleucine degradation	26	1211	56	8202	3.144567654	Bckdha; Hibch; Ehhadh; Aacs; Auh; Aldh6a1; Acat2; Lao1; Dbt; Acaa2; Aox1; Abat; Acaa1a; Hibadh; Oxct1; Mccc2; Aox3; Aldh2; Aox2; Acadsb; Hadh; Echs1; Acaa1b; Hsd17b10; Acadm; Hmgcs1	Bckdha; Hibch; Ehhadh; Aacs; Auh; Aldh6a1; Acat2; Lao1; Dbt; Acaa2; Aox1; Abat; Acaa1a; Hibadh; Oxct1; Mccc2; Aox3; Aldh2; Aox2; Acadsb; Hadh; Echs1; Acaa1b; Hsd17b10; Acadm; Hmgcs1	6.63142E-06	0.000668716
mmu03320	PPAR signaling pathway	33	1211	85	8202	2.629484626	Scd2; Ppara; Acox2; Slc27a4; Plin1; Ehhadh; Acsbg1; Pck1; Acox1; Fabp4; Acaa1a; Sorbs1; Apoc3; Scp2; Acsl3; Acsl1; Apoa1; Fabp6; Acsbg2; Aqp7; Slc27a1; Fads2; Cd36; Cpt1b; Cyp7a1; Gk; Me1; Apoa5; Pparg; Adipoq; Acaa1b; Acadm; Lpl	Scd2; Ppara; Acox2; Slc27a4; Plin1; Ehhadh; Acsbg1; Pck1; Acox1; Fabp4; Acaa1a; Sorbs1; Apoc3; Scp2; Acsl3; Acsl1; Apoa1; Fabp6; Acsbg2; Aqp7; Slc27a1; Fads2; Cd36; Cpt1b; Cyp7a1; Gk; Me1; Apoa5; Pparg; Adipoq; Acaa1b; Acadm; Lpl	8.68463E-06	0.000668716
mmu04146	Peroxisome	32	1211	84	8202	2.580158075	Ech1; Acot8; Acox2; Pipox; Cat; Nudt12; Gnpat; Gstk1; Pex11a; Ehhadh; Pex3; Acox1; Pex5l; Ddo; Eci2; Acaa1a; Baat; Far1; Abcd3; Scp2; Acsl3; Acsl1; Agps; Mvk; Slc25a17; Pxmp2; Pmvk; Mpv17; Pex11g; Acaa1b; Abcd2; Pex16	Ech1; Acot8; Acox2; Pipox; Cat; Nudt12; Gnpat; Gstk1; Pex11a; Ehhadh; Pex3; Acox1; Pex5l; Ddo; Eci2; Acaa1a; Baat; Far1; Abcd3; Scp2; Acsl3; Acsl1; Agps; Mvk; Slc25a17; Pxmp2; Pmvk; Mpv17; Pex11g; Acaa1b; Abcd2; Pex16	1.60908E-05	0.000991195
mmu00982	Drug metabolism - cytochrome	27	1211	68	8202	2.68924564	Maob; Gstk1; Gstm7; Gsto2; Fmo6; Mgst3; Gstt2; Gstt3; Aox1; Gstm5; Cyp2e1; Fmo2; Gsta3; Aox3; Mgst1; Gstm1; Aox2; Maoa; Aldh3a1; Adh7; Fmo4; Adh1; Gstm2; Fmo1; Fmo3; Gsta4; Gsta1	Maob; Gstk1; Gstm7; Gsto2; Fmo6; Mgst3; Gstt2; Gstt3; Aox1; Gstm5; Cyp2e1; Fmo2; Gsta3; Aox3; Mgst1; Gstm1; Aox2; Maoa; Aldh3a1; Adh7; Fmo4; Adh1; Gstm2; Fmo1; Fmo3; Gsta4; Gsta1	4.0974E-05	0.00210333
mmu00640	Propanoate metabolism	17	1211	31	8202	3.714179164	Aldh6a1; Bckdha; Ldhb; Acss2; Dbt; Acat2; Echs1; Suclg2; Hibch; Echdc1; Ehhadh; Abat; Acaca; Acss3; Acadm; Sucla2; Acss1	Aldh6a1; Bckdha; Ldhb; Acss2; Dbt; Acat2; Echs1; Suclg2; Hibch; Echdc1; Ehhadh; Abat; Acaca; Acss3; Acadm; Sucla2; Acss1	5.42577E-05	0.002387339
mmu04024	cAMP signaling pathway	54	1211	197	8202	1.856535061	Camk2a; Atp2b2; Grin2a; Ppara; Sstr1; Fxyd2; Adora1; Lipe; Gria4; Adcy9; Rapgef4; Rapgef3; Cnga1; Tiam1; Nfkbia; Fxyd1; Acox1; Cacna1d; Npy1r; Htr1f; Adcy8; Atp1a1; Pde4c; Pik3r1; Atp1a2; Pde3a; Hcn4; Rock2; Adcy1; Drd2; Gnai1; Rras2; Mapk3; Cacna1c; Gabbr1; Atp1b2; Braf; Mc2r; Gria2; Calm3; Vipr2; Cnga2; Hcn2; Htr1b; Ppp1r1b; Gria3; Calml3; Oxtr; Tshr; Plce1; Adcy3; Gli3; Pln; Camk2b	Camk2a; Atp2b2; Grin2a; Ppara; Sstr1; Fxyd2; Adora1; Lipe; Gria4; Adcy9; Rapgef4; Rapgef3; Cnga1; Tiam1; Nfkbia; Fxyd1; Acox1; Cacna1d; Npy1r; Htr1f; Adcy8; Atp1a1; Pde4c; Pik3r1; Atp1a2; Pde3a; Hcn4; Rock2; Adcy1; Drd2; Gnai1; Rras2; Mapk3; Cacna1c; Gabbr1; Atp1b2; Braf; Mc2r; Gria2; Calm3; Vipr2; Cnga2; Hcn2; Htr1b; Ppp1r1b; Gria3; Calml3; Oxtr; Tshr; Plce1; Adcy3; Gli3; Pln; Camk2b	7.71225E-05	0.002756014
mmu00100	Steroid biosynthesis	13	1211	19	8202	4.6340997	Fdft1; Lss; Hsd17b7; Tm7sf2; Cyp2r1; Dhcr24; Sqle; Cyp51; Sc5d; Msmo1; Nsdhl; Dhcr7; Ebp	Fdft1; Lss; Hsd17b7; Tm7sf2; Cyp2r1; Dhcr24; Sqle; Cyp51; Sc5d; Msmo1; Nsdhl; Dhcr7; Ebp	8.05329E-05	0.002756014

mmu04015	Rap1 signaling pathway	55	1211	209	8202	1.782346039	Prkca; Magi2; Grin2a; Prkd1; Adcy9; Rapgef4; Sipa1l1; Tiam1; Pfn3; Rala; Pard6g; Egf; Adcy8; Pard3; Farp2; Crkl; Flt4; Pgf; P2ry1; Efna3; Pik3r1; Fgf6; Adcy1; Drd2; Insr; Gnai1; Kras; Mapk3; Fgf7; Cdh1; Map2k6; Pard6b; Plcb1; Fgf18; Mras; Id1; Braf; Kdr; Calm3; Rapgef5; Vegfa; Hras; Mapk12; Fgf4; Prkci; Gnao1; Calml3; Plcb4; Plce1; Fgf1; Pdgfd; Rapgef6;	Prkca; Magi2; Grin2a; Prkd1; Adcy9; Rapgef4; Sipa1l1; Tiam1; Pfn3; Rala; Pard6g; Egf; Adcy8; Pard3; Farp2; Crkl; Flt4; Pgf; P2ry1; Efna3; Pik3r1; Fgf6; Adcy1; Drd2; Insr; Gnai1; Kras; Mapk3; Fgf7; Cdh1; Map2k6; Pard6b; Plcb1; Fgf18; Mras; Id1; Braf; Kdr; Calm3; Rapgef5; Vegfa; Hras; Mapk12; Fgf4; Prkci; Gnao1; Calml3; Plcb4; Plce1; Fgf1; Pdgfd; Rapgef6; Adcy3; Rapgef3; Vegfc	0.00016291	0.005017617
P-Steel blue										
mmu05144	Malaria	3	11	55	8202	40.67107438	Hbb-b1; Hba-a1; Gypa	Hbb-b1; Hba-a1; Gypa	5.29837E-05	0.00143056
mmu00910	Nitrogen metabolism	2	11	17	8202	87.72192513	Car1; Car2	Car1; Car2	0.000275449	0.003718561
mmu05143	African trypanosomiasis	2	11	36	8202	41.42424242	Hbb-b1; Hba-a1	Hbb-b1; Hba-a1	0.001116782	0.010051041
mmu04640	Hematopoietic cell lineage	2	11	94	8202	15.86460348	Gypa; Gp9	Gypa; Gp9	0.00694331	0.046867342
mmu04964	Proximal tubule bicarbonate reclamation	1	11	22	8202	33.89256198	Car2	Car2	0.030395341	0.16413484
mmu04966	Collecting duct acid secretion	1	11	27	8202	27.61616162	Car2	Car2	0.036890842	0.164605079
mmu04216	Ferroptosis	1	11	39	8202	19.11888112	Alox15	Alox15	0.052318962	0.164605079
mmu00260	Glycine, serine and threonine metabolism	1	11	40	8202	18.64090909	Alas2	Alas2	0.053594441	0.164605079
mmu00860	Porphyrin and chlorophyll metabolism	1	11	41	8202	18.18625277	Alas2	Alas2	0.05486836	0.164605079
mmu00591	Linoleic acid	1	11	50	8202	14.91272727	Alox15	Alox15	0.066263673	0.178053448
P-White										
mmu00072	Synthesis and degradation of ketone bodies	1	7	11	8202	106.5194805	Hmgcs2	Hmgcs2	0.010191615	0.133625473
mmu00900	Terpenoid backbone biosynthesis	1	7	23	8202	50.94409938	Hmgcs2	Hmgcs2	0.020294069	0.133625473
mmu00650	Butanoate metabolism	1	7	27	8202	43.3968254	Hmgcs2	Hmgcs2	0.023641853	0.133625473
mmu04614	Renin-angiotensin system	1	7	36	8202	32.54761905	Enpep	Enpep	0.031138534	0.133625473

mmu00280	Valine, leucine and isoleucine degradation	1	7	56	8202	20.92346939	Hmgcs2	Hmgcs2	0.047621385	0.133625473
mmu00480	Glutathione metabolism	1	7	61	8202	19.20843091	Gsr	Gsr	0.051704335	0.133625473
mmu00010	Glycolysis / Gluconeogenesis	1	7	68	8202	17.23109244	Gapdh	Gapdh	0.057395254	0.133625473
mmu04918	Thyroid hormone synthesis	1	7	73	8202	16.05088063	Gsr	Gsr	0.061442251	0.133625473
mmu03320	PPAR signaling pathway	1	7	85	8202	13.78487395	Hmgcs2	Hmgcs2	0.071094329	0.133625473
mmu04540	Gap junction	1	7	86	8202	13.62458472	Tuba3a	Tuba3a	0.071894814	0.133625473
D-Blue										
mmu04974	Protein digestion and absorption	28	807	90	8202	3.161999174	Cela3b; Col4a4; Slc3a1; Col9a1; Slc38a2; Slc9a3; Col4a5; Atp1b3; Col4a2; Slc15a1; Atp1a2; Col1a1; Slc8a3; Col9a2; Slc8a2; Atp1b2; Cpa3; Col2a1; Col24a1; Ace2; Col9a3; Col5a3; Fxyd2; Ctrl; Atp1a1; Mme; Col10a1; Slc1a5	Cela3b; Col4a4; Slc3a1; Col9a1; Slc38a2; Slc9a3; Col4a5; Atp1b3; Col4a2; Slc15a1; Atp1a2; Col1a1; Slc8a3; Col9a2; Slc8a2; Atp1b2; Cpa3; Col2a1; Col24a1; Ace2; Col9a3; Col5a3; Fxyd2; Ctrl; Atp1a1; Mme; Col10a1; Slc1a5	1.18568E-06	0.000356891
mmu00100	Steroid biosynthesis	11	807	19	8202	5.884171395	Dhcr24; Ebp; Msmo1; Nsdhl; Cyp51; Sc5d; Hsd17b7; Fdft1; Sqle; Tm7sf2; Lss	Dhcr24; Ebp; Msmo1; Nsdhl; Cyp51; Sc5d; Hsd17b7; Fdft1; Sqle; Tm7sf2; Lss	3.09267E-05	0.004654473
mmu04261	Adrenergic signaling in cardiomyocytes	33	807	147	8202	2.28161748	Adrb2; Mapk3; Cacnb4; Cacng5; Adcy3; Scn7a; Rapgef3; Ryr2; Atp1b3; Atp1a2; Ppp2r3a; Rps6ka5; Adra1b; Tnnt2; Myh6; Ppp2r2c; Atp2b2; Gnai1; Creb3l1; Myh7; Atp1b2; Cacng4; Ppp2r2b; Camk2b; Tnnc1; Cacna1s; Cacng8; Fxyd2; Cacnb3; Plcb1; Atp1a1; Cacna1c; Myl2	Adrb2; Mapk3; Cacnb4; Cacng5; Adcy3; Scn7a; Rapgef3; Ryr2; Atp1b3; Atp1a2; Ppp2r3a; Rps6ka5; Adra1b; Tnnt2; Myh6; Ppp2r2c; Atp2b2; Gnai1; Creb3l1; Myh7; Atp1b2; Cacng4; Ppp2r2b; Camk2b; Tnnc1; Cacna1s; Cacng8; Fxyd2; Cacnb3; Plcb1; Atp1a1; Cacna1c; Myl2	5.0857E-05	0.005041956
mmu00280	Valine, leucine and isoleucine degradation	18	807	56	8202	3.266861391	Pccb; Abat; Aldh6a1; Aldh2; Mccc2; Acaa2; Aldh3a2; Hmgcs2; Pcca; Acat2; Dbt; Acaa1b; Aacs; Oxct2a; Aox1; Hmgcs1; Acaa1a; Aox4	Pccb; Abat; Aldh6a1; Aldh2; Mccc2; Acaa2; Aldh3a2; Hmgcs2; Pcca; Acat2; Dbt; Acaa1b; Aacs; Oxct2a; Aox1; Hmgcs1; Acaa1a; Aox4	6.70027E-05	0.005041956
mmu00900	Terpenoid backbone biosynthesis	11	807	23	8202	4.860837239	Fdps; Mvd; Hmgcs2; Hmgcr; Acat2; Hmgcs1; Fntb; Pmvk; Mvk; Idi1; Fnta	Fdps; Mvd; Hmgcs2; Hmgcr; Acat2; Hmgcs1; Fntb; Pmvk; Mvk; Idi1; Fnta	0.000115983	0.006513654
mmu00062	Fatty acid elongation	12	807	28	8202	4.355815189	Hacd3; Acot2; Acaa2; Elovl6; Elovl5; Tecr; Elovl1; Elovl4; Hacd1; Them4; Hacd4; Hacd2	Hacd3; Acot2; Acaa2; Elovl6; Elovl5; Tecr; Elovl1; Elovl4; Hacd1; Them4; Hacd4; Hacd2	0.00012984	0.006513654
mmu00380	Tryptophan metabolism	15	807	46	8202	3.314207209	Ogdh; Kynu; Aldh2; Maoa; Aldh3a2; Acat2; Gcdh; Aanat; Tdo2; Aox1; Aadat; Aox4; Maob; Cyp1a1; Inmt	Ogdh; Kynu; Aldh2; Maoa; Aldh3a2; Acat2; Gcdh; Aanat; Tdo2; Aox1; Aadat; Aox4; Maob; Cyp1a1; Inmt	0.000234809	0.009419685
mmu04727	GABAergic synapse	22	807	88	8202	2.540892193	Abat; Plcl1; Adcy3; Kcnj6; Gabbr1; Slc38a2; Hap1; Slc32a1; Gng2; Gabarapl1; Gabarapl2; Gnai1; Slc38a5; Gng3; Gnb3; Gls2; Cacna1s; Slc38a3; Gng7; Gabrb1; Cacna1c; Gabra3	Abat; Plcl1; Adcy3; Kcnj6; Gabbr1; Slc38a2; Hap1; Slc32a1; Gng2; Gabarapl1; Gabarapl2; Gnai1; Slc38a5; Gng3; Gnb3; Gls2; Cacna1s; Slc38a3; Gng7; Gabrb1; Cacna1c; Gabra3	0.000250357	0.009419685
mmu04713	Circadian entrainment	23	807	98	8202	2.385327365	Mapk3; Adcy3; Kcnj6; Per2; Ryr2; Ryr3; Nos1; Rps6ka5; Ryr1; Gng2; Gnai1; Per1; Gng3; Gnb3; Camk2b; Grin2b; Grin2a; Rasd1; Gng7; Kcnj5; Plcb1; Cacna1c; Nos1ap	Mapk3; Adcy3; Kcnj6; Per2; Ryr2; Ryr3; Nos1; Rps6ka5; Ryr1; Gng2; Gnai1; Per1; Gng3; Gnb3; Camk2b; Grin2b; Grin2a; Rasd1; Gng7; Kcnj5; Plcb1; Cacna1c; Nos1ap	0.000397317	0.01328805

mmu01040	Biosynthesis of unsaturated fatty acids	11	807	28	8202	3.992830589	Hacd3; Baat; Acot2; Elovl6; Elovl5; Tecr; Acaa1b; Hacd1; Acaa1a; Hacd4; Hacd2	Hacd3; Baat; Acot2; Elovl6; Elovl5; Tecr; Acaa1b; Hacd1; Acaa1a; Hacd4; Hacd2	0.000448196	0.013490705
D-Salmon										
mmu04966	Collecting duct acid secretion	2	19	27	8202	31.97660819	Slc4a1; Car2	Slc4a1; Car2	0.00197967	0.106902155
mmu00860	Porphyrin and chlorophyll metabolism	2	19	41	8202	21.05776637	Alas2; Fech	Alas2; Fech	0.004319048	0.116614294
mmu04640	Hematopoietic cell lineage	2	19	94	8202	9.184770437	Gypa; Itga2b	Gypa; Itga2b	0.020280796	0.365054335
mmu04080	Neuroactive ligand-receptor interaction	3	19	312	8202	4.150809717	Crhr2; F2; Avpr1b	Crhr2; F2; Avpr1b	0.034252755	0.375275873
mmu00910	Nitrogen metabolism	1	19	17	8202	25.39318885	Car2	Car2	0.040834937	0.375275873
mmu04964	Proximal tubule bicarbonate reclamation	1	19	22	8202	19.62200957	Car2	Car2	0.051894496	0.375275873
mmu04950	Maturity onset diabetes of the young	1	19	27	8202	15.98830409	Pdx1	Pdx1	0.062833173	0.375275873
mmu05034	Alcoholism	2	19	199	8202	4.338534779	Npy; Hist1h2ba	Npy; Hist1h2ba	0.077484638	0.375275873
mmu04810	Regulation of actin cytoskeleton	2	19	210	8202	4.111278195	Itga2b; F2	Itga2b; F2	0.084945449	0.375275873
mmu04216	Ferroptosis	1	19	39	8202	11.06882591	Alox15	Alox15	0.08860024	0.375275873
D-Purple										
mmu04668	TNF signaling pathway	18	76	108	8202	17.98684211	Socs3; Birc3; Il6; Cebpb; Junb; Cflar; Map3k8; Ccl20; Cxcl2; Ptgs2; Fos; Cxcl1; Icam1; Map3k14; Tnf; Il1b; Birc2; Nfkbia	Socs3; Birc3; Il6; Cebpb; Junb; Cflar; Map3k8; Ccl20; Cxcl2; Ptgs2; Fos; Cxcl1; Icam1; Map3k14; Tnf; Il1b; Birc2; Nfkbia	3.32397E-17	5.85019E-15
mmu04657	IL-17 signaling pathway	12	76	91	8202	14.2313476	S100a9; Il6; Cebpb; Ccl20; Cxcl2; Ptgs2; Fos; Cxcl1; Il1b; Tnf; Nfkbia; S100a8	S100a9; Il6; Cebpb; Ccl20; Cxcl2; Ptgs2; Fos; Cxcl1; Il1b; Tnf; Nfkbia; S100a8	1.14941E-10	1.01148E-08
mmu04064	NF-kappa B signaling pathway	12	76	102	8202	12.69659443	Birc3; Gadd45b; Cflar; Cxcl2; Ptgs2; Icam1; Map3k14; Il1b; Tnf; Birc2; Nfkbia; Plau	Birc3; Gadd45b; Cflar; Cxcl2; Ptgs2; Icam1; Map3k14; Il1b; Tnf; Birc2; Nfkbia; Plau	3.83458E-10	2.24962E-08
mmu04210	Apoptosis	11	76	136	8202	8.728908669	Birc3; Ngf; Gadd45b; Gadd45g; Cflar; Mcl1; Map3k14; Fos; Tnf; Birc2; Nfkbia	Birc3; Ngf; Gadd45b; Gadd45g; Cflar; Mcl1; Map3k14; Fos; Tnf; Birc2; Nfkbia	8.10421E-08	3.56585E-06
mmu04010	MAPK signaling pathway	14	76	294	8202	5.139097744	Ngf; Dusp1; Gadd45b; Gadd45g; Myc; Map3k8; Fgf17; Dusp2; Hspa1a; Fos; Map3k14; Dusp5; Il1b; Tnf	Ngf; Dusp1; Gadd45b; Gadd45g; Myc; Map3k8; Fgf17; Dusp2; Hspa1a; Fos; Map3k14; Dusp5; Il1b; Tnf	6.20445E-07	2.18396E-05
mmu05134	Legionellosis	7	76	58	8202	13.02495463	Il6; Cxcl2; Hspa1a; Il1b; Cxcl1; Tnf; Nfkbia	Il6; Cxcl2; Hspa1a; Il1b; Cxcl1; Tnf; Nfkbia	1.88797E-06	5.53804E-05

mmu05222	Small cell lung cancer	8	76	92	8202	9.384439359	Birc3; Gadd45b; Gadd45g; Myc; Ptgs2; Nos2; Birc2; Nfkbia	Birc3; Gadd45b; Gadd45g; Myc; Ptgs2; Nos2; Birc2; Nfkbia	3.27708E-06	8.23951E-05
mmu05142	Chagas disease (American trypanosomiasis)	8	76	101	8202	8.548202189	Il6; Cflar; Fos; Nos2; Il1b; Tnf; Nfkbia; Serpine1	Il6; Cflar; Fos; Nos2; Il1b; Tnf; Nfkbia; Serpine1	6.26251E-06	0.000137775
mmu05202	Transcriptional misregulation in cancers	10	76	183	8202	5.89732528	Birc3; Il6; Cebpb; Gadd45b; Gadd45g; Myc; Nfkbiz; Il1r2; Nr4a3; Plau	Birc3; Il6; Cebpb; Gadd45b; Gadd45g; Myc; Nfkbiz; Il1r2; Nr4a3; Plau	9.42494E-06	0.00018431
mmu05166	HTLV-I infection	12	76	281	8202	4.608728226	Ets2; Il6; Zfp36; Myc; Il1r2; Map3k14; Icam1; Fos; Tnf; Crem; Nfkbia; Egr1	Ets2; Il6; Zfp36; Myc; Il1r2; Map3k14; Icam1; Fos; Tnf; Crem; Nfkbia; Egr1	1.25886E-05	0.00022156

KEGG: Kyoto Encyclopedia of Genes and Genomes.